nature immunology

Pre-existing clusters of the adaptor Lat do not participate in early T cell signaling events

David J Williamson[1,3], Dylan M Owen[1,3], Jérémie Rossy[1,3], Astrid Magenau[1], Matthias Wehrmann[2], J Justin Gooding[2] & Katharina Gaus[1]

Engaged T cell antigen receptors (TCRs) initiate signaling through the adaptor protein Lat. In quiescent T cells, Lat is segregated into clusters on the cell surface, which raises the question of how TCR triggering initiates signaling. Using super-resolution fluorescence microscopy, we found that pre-existing Lat domains were neither phosphorylated nor laterally transported to TCR activation sites, which suggested that these clusters do not participate in TCR signaling. Instead, TCR activation resulted in the recruitment and phosphorylation of Lat from subsynaptic vesicles. Studies of Lat mutants confirmed that recruitment preceded and was essential for phosphorylation and that both processes were independent of surface clustering of Lat. Our data suggest that TCR ligation preconditions the membrane for vesicle recruitment and bulk activation of the Lat signaling network.

T cell activation and the establishment of an immunological synapse[1] involve the spatio-temporal arrangement of signaling molecules into microclusters[2,3], condensation of the plasma membrane[4,5] and rearrangement of the actin cytoskeleton[6,7]. The T cell antigen receptor (TCR) recognizes processed antigenic peptides, which establishes TCR complexes and supramolecular activation clusters[8,9]. Subunits of the receptor complex are phosphorylated by the kinase Lck[10,11] and serve as recruitment and activation sites for the T cell signaling protein Zap70. Zap70 in turn phosphorylates additional signaling proteins, including the adaptor Lat (linker for activation of T cells)[12].

Lat is a transmembrane adaptor protein that is essential for TCR signaling[13], T cell activation[14] and development[15]. Lat lacks any intrinsic enzymatic activity but serves as a platform for several adaptor and effector molecules. These interactions of phosphorylated Lat trigger downstream signaling cascades that drive gene expression and cytokine secretion[13,14]. Hence, the assembly of Lat signaling complexes is a critical step in the early T cell signaling response[16,17]. However, insights into the molecular mechanisms of TCR-induced reorganization of Lat have been limited by the resolution of fluorescence microscopes.

Total internal reflection fluorescence (TIRF) microscopy has shown that TCR microclusters continuously form at the periphery of the synapse[2,3]; they are actively transported from there to the central region[6] by processes dependent on actin[7] and myosin II[18]. At the center, it is thought that signaling is terminated[19] and the receptor is internalized[20]. Studies using super-resolution fluorescence microscopy have found that in the plasma membranes of resting T cells, the TCR and Lat already exist in discrete clusters 70–140 nm in diameter[21]. These clusters remained separated during T cell activation, which raises the question of how TCR triggering results in the phosphorylation of Lat and hence the initiation of early T cell signaling responses.

Here we systematically compared Lat clustering in resting and activated T cells by photo-activatable localization microscopy (PALM)[22,23] and direct stochastic optical reconstruction microscopy (dSTORM)[24,25], each with quantitative statistical cluster analysis. We found that the observed increase in Lat clusters after T cell stimulation was the result of the translocation of subsynaptic Lat-containing vesicles to the cell surface. That recruitment was independent of surface-crosslinked Lat, and Lat mutants that impaired vesicular trafficking were neither recruited nor phosphorylated. This was because mainly newly recruited clusters of Lat, rather than pre-existing Lat domains in the plasma membrane, were phosphorylated after TCR triggering. Our data suggest that Lat signaling networks are established *en masse* by docking of vesicles at the plasma membrane and not by Lat reorganization within the plasma membrane. This mechanism indicates that intracellular compartments and vesicles have a controlling role in the regulation of TCR signaling. Such a 'plug-and-signal' model may explain the rapid onset of TCR signaling and extreme signal amplification that is characteristic of the T cell system.

RESULTS

Lat PALM and cluster mapping

We expressed wild-type human Lat fused at the carboxyl terminus to the photoactivatable fluorescent protein mEos2 (Lat-mEos2) in the Lat-deficient Jurkat human T lymphocyte cell line JCaM2. For activation, we incubated cells for 10 min with coverslips coated with antibody to CD3 (anti-CD3) and anti-CD28 and fixed the cells in paraformaldehyde. We fixed resting T cells in suspension and attached them onto uncoated coverslips by centrifugation (**Supplementary Figs. 1–3**).

We imaged and analyzed resting and activated Lat-expressing JCaM2 cells by TIRF microscopy and PALM (**Fig. 1**). We observed higher Lat

[1]Centre for Vascular Research, University of New South Wales, Sydney, Australia. [2]School of Chemistry and the Australian Centre for Nanomedicine, University of New South Wales, Sydney, Australia. [3]These authors contributed equally to this work. Correspondence should be addressed to K.G. (k.gaus@unsw.edu.au).

Received 25 February; accepted 5 May 2011; published online 5 June 2011; doi:10.1038/ni.2049

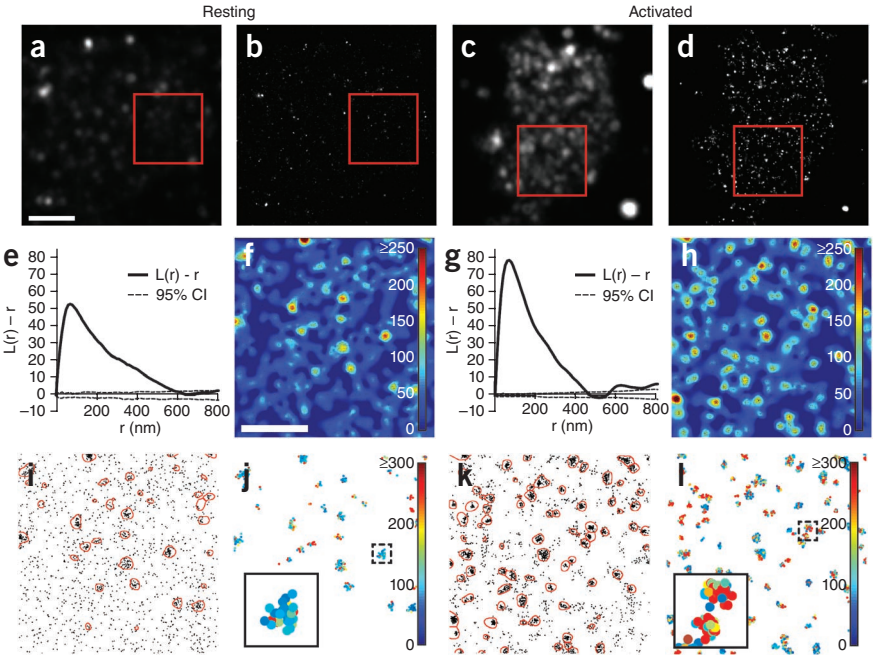

Figure 1 Mapping of single Lat molecules in resting and activated T cells. (**a**–**d**) TIRF images (**a**,**c**) and single-molecule PALM images (**b**,**d**) of adherent Lat-deficient JCaM2 cells transfected with a plasmid expressing Lat-mEos2 and fixed in suspension (Resting) or exposed for 10 min to glass coverslips coated with anti-CD3 and anti-CD28 (Activated). Scale bar, 2 μm. (**e**) Ripley's K-function analysis of the molecules in regions outlined in red in **a**,**b**; L(r)—r reports the degree of clustering relative to a random distribution (indicated by the 95% confidence interval (CI)), and r is the radial scale. (**f**) Lat cluster maps of the regions outlined in **a**,**b**, generated from local point-pattern analysis. (**g**) Ripley's K-function analysis as in **e** for regions outlined in red in **c**,**d**. (**h**) Lat cluster maps as in **f**, for regions outlined in **c**,**d**. Color (**f**,**h**) indicates clustering (L(r)), from low (blue) to high (red); scale bar, 1 μm. (**i**) Map of regions outlined in red in **a**,**b** containing all Lat molecules and Lat clusters identified after application of a clustering threshold. (**j**) Map of clustered Lat molecules in **a**,**b**; colors indicate photons emitted per molecule. (**k**) Map of Lat molecules and clusters as in **i**, for regions in **c**,**d**. (**l**) Maps of clustered Lat molecules as in **j**, for regions in **c**,**d**. Inset (**j**,**l**), clusters of Lat (dashed outline in main image) at fourfold higher magnification; main image size (**i**–**l**), 3 μm × 3 μm. Data are representative of 20–25 experiments.

concentrations at the cell surface on activated T cells than on resting T cells, as indicated by the higher intensity and greater molecular density, respectively, by both TIRF (**Fig. 1a**,**c**) and PALM (**Fig. 1b**,**d**). We analyzed the distribution of Lat by Ripley's K function (**Fig. 1e**,**g**). These plots showed that Lat was clustered even in nonactivated T cells, as reported before[21]. Although the radial scale of peak clustering was not affected much by activation, Lat was more clustered in activated cells than resting cells. Pseudo-colored cluster maps showed that there were more clusters of Lat after activation, whereas the cluster size seemed similar (**Fig. 1f**,**h**). We applied a threshold to show that clusters of Lat existed in resting T cells and that the number of clusters of Lat was greater after TCR triggering (**Fig. 1i**,**k**).

As well as providing the molecular coordinates, the Gaussian fitting algorithm of PALM also provided the number of collected photons for each molecule (**Supplementary Fig. 1**). Because the strength of the TIRF evanescent field decays exponentially with distance from the interface, the number of collected photons tends to be greater for molecules in the plasma membrane[26]. We applied a pseudo-color map to each clustered Lat molecule on the basis of the number of collected photons (**Fig. 1j**,**l**). In resting cells, a large proportion of clusters of Lat contained molecules with a relatively low photon count (blue, **Fig. 1j**), which suggested that molecules resided some distance away from the plasma membrane, possibly in submembrane vesicles. In activated cells, we observed more clusters that contained molecules with a high photon count (red, **Fig. 1l**). These images indicate that after activation, clusters of Lat translocate closer to the plasma membrane.

The statistics of Lat-cluster properties showed that the number of clusters per μm^2 of membrane increased over twofold with activation, from 4.2 ± 1.0 (mean ± s.d.) clusters per μm^2 in resting cells to 9.0 ± 1.0 clusters per μm^2 after activation (**Fig. 2a**). Notably, the average number of Lat molecules per cluster was only slightly greater in activated T cells (43.9 ± 8.0 molecules per cluster) than in resting T cells (28.5 ± 18.0 molecules per cluster; $P = 0.0344$), and clusters of Lat remained round in shape in activated T cells (circularity: 0.81 ± 0.09 in activated cells versus 0.81 ± 0.09 in resting cells; $P = 0.13$), which suggested that the underlying mechanism of Lat clustering may have been similar under both conditions. The TCR-induced increase in Lat clusters was only moderately driven by the recruitment of monomeric Lat into clusters, as the percentage of Lat molecules that contribute to clusters increased only 1.5-fold, from 39.3% ± 12.0% in resting cells to 58.2% ± 11.8% in activated cells (**Fig. 2b**). In contrast, the total Lat concentration increased substantially, from 266.1 ± 63.0 Lat molecules per μm^2 in resting cells to 723.5 ± 251.8 Lat molecules per μm^2 after TCR triggering (**Fig. 2c**), a 2.7-fold increase consistent with the greater intensity in the TIRF and PALM images (**Fig. 1**). These data suggest that TCR activation results in the recruitment of predominately clustered Lat molecules. Hence, aggregation of Lat monomers in the plasma membrane is probably not the main mechanism of TCR-induced Lat clustering.

Next we attempted to identify clusters formed from newly recruited Lat molecules in activated T cells. To do so, we examined the size distributions of Lat clusters in more detail (**Fig. 2d**). The mean cluster size was not significantly different after activation, with clusters in resting and activated cells having diameters of 117.2 nm ± 49.1 nm and 112.7 nm ± 40.4 nm, respectively ($P = 0.993$). However, the distributions of cluster sizes in these two conditions, as analyzed by nonlinear curve fitting, were significantly different. We identified a distinct subpopulation of Lat clusters in activated cells that was less abundant in resting cells (**Fig. 2d**, inset). This population of TCR-induced clusters of Lat had an area between 5,000 nm^2 and 16,000 nm^2 and a diameter ranging from 80 nm to 140 nm. Therefore, the new clusters of Lat that appeared after activation were probably a distinct subpopulation of Lat clusters with a mainly intermediate size. The distribution of photon counts showed that a greater proportion of Lat molecules emitted more photons in activated cells than in resting cells (**Fig. 2e**). This indicated that newly recruited Lat molecules were closer to the cell-coverslip interface in activated cells than in resting cells. Together these results suggest a model in

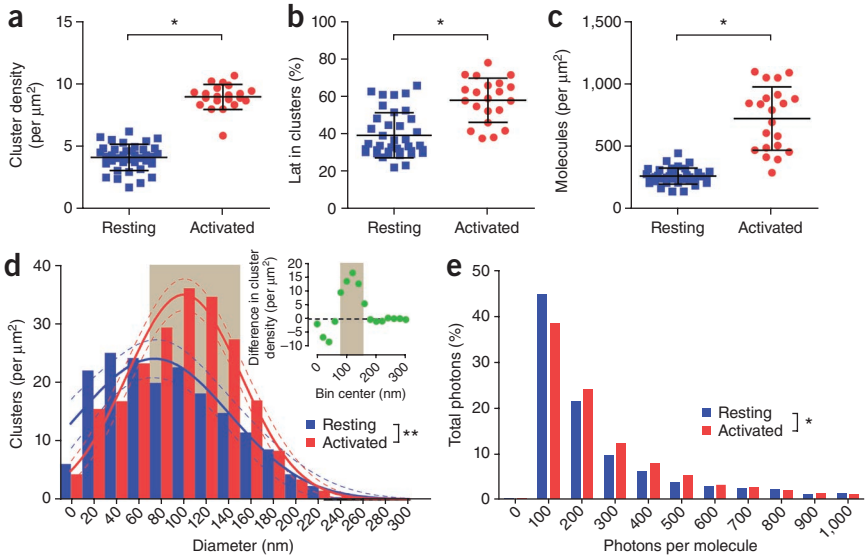

Figure 2 Quantitative statistical analysis of Lat clustering in resting and activated T cells. (**a**–**c**) Lat clusters per μm^2 (**a**), frequency of Lat in clusters (**b**) and total density of Lat (**c**) obtained from PALM data after local point-pattern analysis and application of a cluster threshold in resting and activated JCaM2 cells expressing Lat-mEos2. Each symbol represents one image region; horizontal bars and error bars indicate mean and s.d., respectively (throughout). $*P < 0.0001$ (Student's *t*-test). (**d**,**e**) Distribution of the size of Lat clusters (**d**) and of photons emitted from each Lat molecule (**e**) obtained by analysis PALM image regions with local point-pattern analysis and application of a cluster threshold in resting ($n = 38$ regions) and activated ($n = 21$ regions) JCaM2 cells expressing Lat-mEos2. In **d**, distributions were analyzed by nonlinear curve fitting (solid lines) with 95% confidence intervals (dashed lines); shaded tan area indicates significant difference. Inset (**d**), Difference between resting and activated cells in cluster size distribution. $*P < 0.01$ and $**P < 0.0001$ (Student's *t*-test). Data are representative of 20–25 experiments.

which TCR activation results in the recruitment of clustered Lat from vesicular pools to the plasma membrane.

Clustering of endogenous Lat and phosphorylated Lat

We examined the distribution of endogenous and phosphorylated Lat in Lat-expressing wild-type Jurkat cells and primary naive T cells by dSTORM and immunostaining. A consequence of using antibodies conjugated to fluorophores that can cycle between dark and fluorescent states is the repeated detection of labeled molecules[24]. We minimized this effect by ignoring fluorescent events that localized to the same position within 50 frames of the first event (**Supplementary Fig. 1e**,**f**). Cluster analysis of dSTORM images indicated that 58.4% ± 8.6% of endogenous Lat molecules were monomeric in resting T cells, in agreement with the PALM data (**Fig. 2b**).

Cluster maps (**Fig. 3a**) and the corresponding Ripley's K-function plots (**Fig. 3b**) demonstrated a higher percentage of molecules in clusters of phosphorylated Lat than of total Lat (67.7% ± 11.1 and 41.6% ± 8.6, respectively; **Fig. 3c**) in activated Jurkat cells. This further confirmed our cluster analysis, as few phosphorylated Lat molecules are monomeric[27]. Clusters of total Lat were

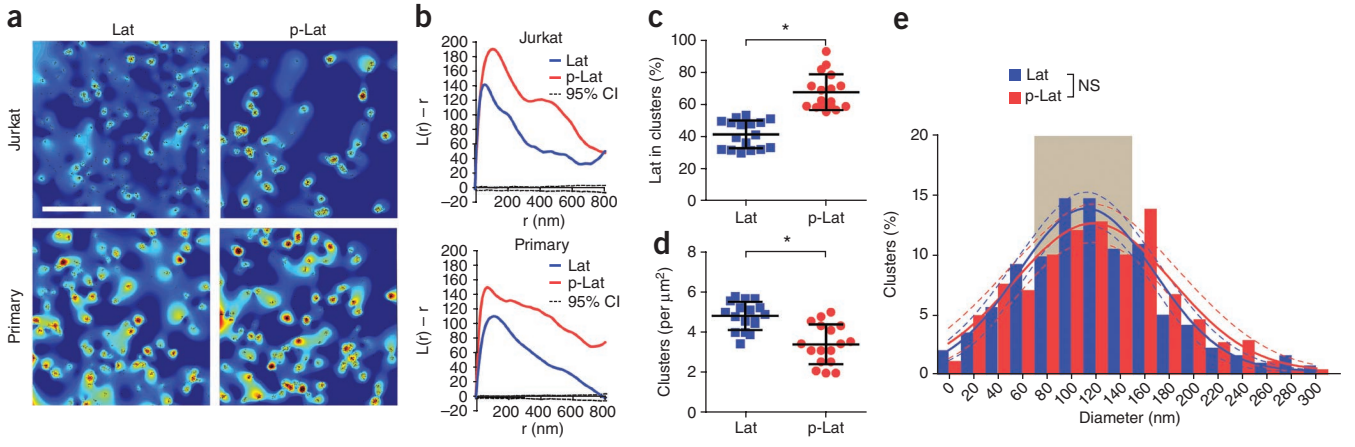

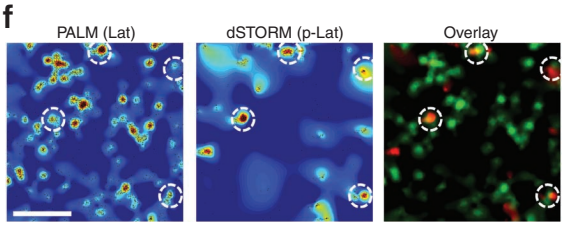

Figure 3 Clustering of endogenous Lat and phosphorylated Lat in activated wild-type Jurkat cells and primary mouse T cells. (**a**,**b**) Cluster maps (**a**) and Ripley's K-function plots (**b**) of dSTORM images of endogenous Lat and phosphorylated Lat (p-Lat) in activated Jurkat cells (top) and primary mouse T cells (bottom), obtained by local point-pattern analysis. Scale bar (**a**), 1 µm. (**c**,**d**) Quantification of the frequency of Lat and phosphorylated Lat in clusters (**c**) and cluster counts per μm^2 (**d**) in Jurkat cells, obtained by analysis of dSTORM image regions with local point-pattern analysis and application of a cluster threshold. $*P < 0.0001$ (Student's *t*-test). (**e**) Distribution of cluster sizes for Lat ($n = 11$) and phosphorylated Lat ($n = 12$) in image regions in activated Jurkat cells, obtained as in **c**,**d**. Shaded tan area indicates the size range in which new Lat clusters appeared after TCR activation, as detected by PALM in JCaM2 cells expressing Lat-mEos2. NS, not significant ($P > 0.05$). (**f**) Dual-channel analysis of Lat (PALM; green in merged image) and phosphorylated Lat (dSTORM; red in merged image) in an image region in an activated wild-type Jurkat cell. Dashed white circles outline regions in which Lat and phosphorylated Lat clusters overlap. Scale bar, 1 µm. Data are representative of 10–15 experiments.

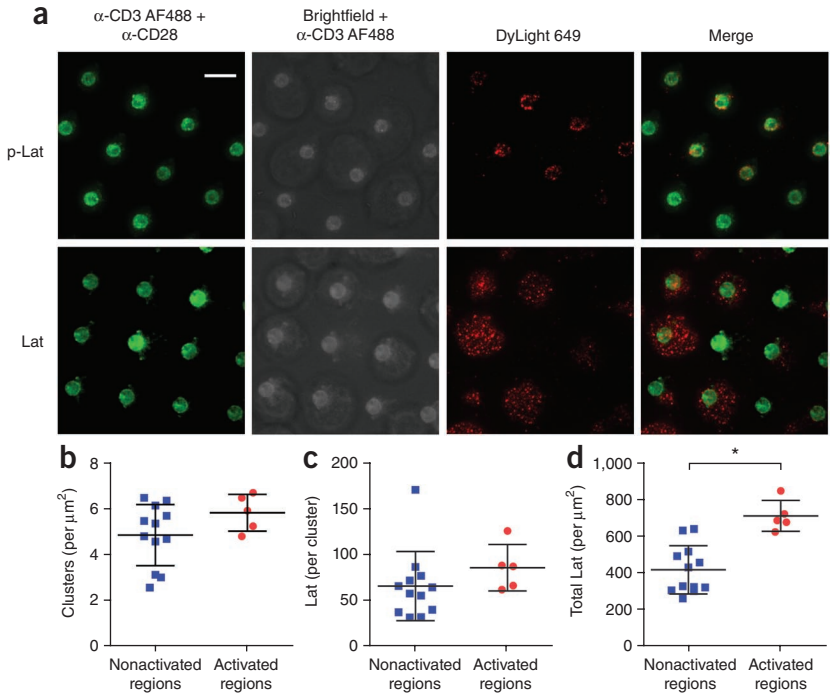

Figure 4 Localized activation of T cells on micro-patterned surfaces. (**a**) TIRF and brightfield images of wild-type Jurkat cells incubated for 10 min with glass surfaces onto which Alexa Fluor 488 (AF488)-conjugated anti-CD3 and anti-CD28 were micro-patterned, followed by immunostaining with DyLight649-conjugated antibody to phosphorylated Lat or to total Lat. Scale bar, 10 μm. (**b**–**d**) Quantification of Lat clusters per μm^2 (**b**), Lat molecules per cluster (**c**) and total Lat density (**d**) in nonactivated and activated regions from the wild-type Jurkat cells in **a**, obtained by analysis of dSTORM image regions by local point-pattern analysis and application of a cluster threshold. *$P < 0.001$ (Student's *t*-test). Data are representative of five to eight experiments.

significantly more abundant than were clusters of phosphorylated Lat (4.8 ± 0.7 per μm^2 and 3.1 ± 1.0 per μm^2, respectively; **Fig. 3d**). Notably, this difference in cluster count was similar to the difference between resting and activated cells (**Fig. 2a**), which suggested that newly recruited clusters may be mostly phosphorylated. We found no phosphorylated Lat in resting cells, which indicated that pre-existing clusters of Lat are not sufficient to induce phosphorylation.

Next we analyzed the size distributions of clusters of total and phosphorylated Lat and found no significant difference (**Fig. 3e**). Hence, the population of clusters of phosphorylated Lat in activated T cells and TCR-induced clusters of Lat were identical in terms of size distribution, with the diameter of clusters of phosphorylated Lat (117–127 nm; **Fig. 3e**) being in the size range of TCR-induced clusters of Lat observed by PALM (80–140 nm in diameter; **Fig. 2d**). Therefore, the correlation between the sizes of clusters of Lat and phosphorylated Lat indicated that newly recruited clusters of Lat are mainly phosphorylated after TCR triggering.

If the hypothesis is correct and newly recruited rather than pre-existing clusters of Lat are phosphorylated, two different Lat-cluster populations should coexist in activated T cells; that is, clusters that do and do not contain phosphorylated Lat. Hence, we did dual-channel PALM-dSTORM to identify clusters of total Lat as well as clusters of phosphorylated Lat in activated T cells (**Fig. 3f**). Clustered phosphorylated Lat resided mainly in a discrete subpopulation of Lat clusters, and there were many clusters that did not contain phosphorylated Lat. Clusters in which Lat and phosphorylated Lat did coincide were characterized by an intermediate size range (**Fig. 3f**). These observations indicate that phosphorylation occurs mainly on newly recruited clusters of Lat or vesicles of intermediate size.

Recruitment of clusters of Lat to TCR-activation sites

We next addressed the relationship between pre-existing clusters of Lat and the formation of new TCR-induced clusters of Lat. In particular, we investigated whether Lat is laterally transported to the activation site and whether pre-existing clusters of Lat are disassembled on nonactivated regions of the plasma membrane. To test this, we constructed 'micro-patterned' activation surfaces in which a mixture of anti-CD3 and anti-CD28 was deposited in circles 4 μm in diameter with their centers 14 μm apart (**Fig. 4a**). This geometry ensured that each cell could adhere to only one activation area and allowed us to quantify clustering of Lat at zones of activation and nonactivation in the same cell.

After 10 min of activation on micro-patterned surfaces, phosphorylated Lat was present only in membrane regions that were in contact with the antibody activation zone, whereas Lat was present across the entire membrane interface (**Fig. 4a**). These images confirmed that TCR activation was restricted to the antibody pattern. To address whether Lat was transported laterally, we measured radial intensity profiles from the center of the activating dots to nonactivating regions (**Supplementary Fig. 4**). As expected, the concentration of Lat was higher on activated regions, as Lat was recruited to these sites. However, we did not find any accumulation of Lat at the interface between nonactivated and activated regions, as we did for F-actin. F-actin is transported laterally to the activation site[7] and becomes arrested by the adherent antibodies, which results in a buildup of molecules at the interface. This suggested that surface Lat is not recruited laterally to the activation site.

To determine whether pre-existing clusters of Lat are disassembled, we applied the dSTORM approach to Lat on nonactivated and activated regions. Unlike activating surfaces that were completely covered by antibodies, the patterned surfaces did not result in more clusters of Lat (**Fig. 4b**) or more Lat molecules per cluster (**Fig. 4c**). This difference may be explained by the lower number of TCRs per cell that were activated with patterned surfaces than with antibody-coated surfaces. However, the molecular density of Lat was significantly greater on activating areas than on nonactivating areas (711.2 ± 83.1 molecules per μm^2 and 442.0 ± 114.1 molecules per μm^2, respectively; **Fig. 4d**). The number of Lat clusters on nonactivated areas (4.8 ± 1.3 clusters per μm^2) was similar to that in nonactivated Jurkat cells (4.8 ± 0.7 clusters per μm^2; $P > 0.05$), and the percentage of Lat outside clusters was also similar on nonactivated areas (30.7 ± 8.2%) and activated areas (31.7 ± 6.7%; $P > 0.05$). These data indicate that recruitment of clusters of Lat does not occur at the expense of the pre-existing clusters of Lat and hence it is unlikely that such pre-existing clusters are disassembled. Instead, the increase in Lat molecules at the TCR activation site may have been due to recruitment of Lat from outside the TIRF zone, such as from an intracellular pool.

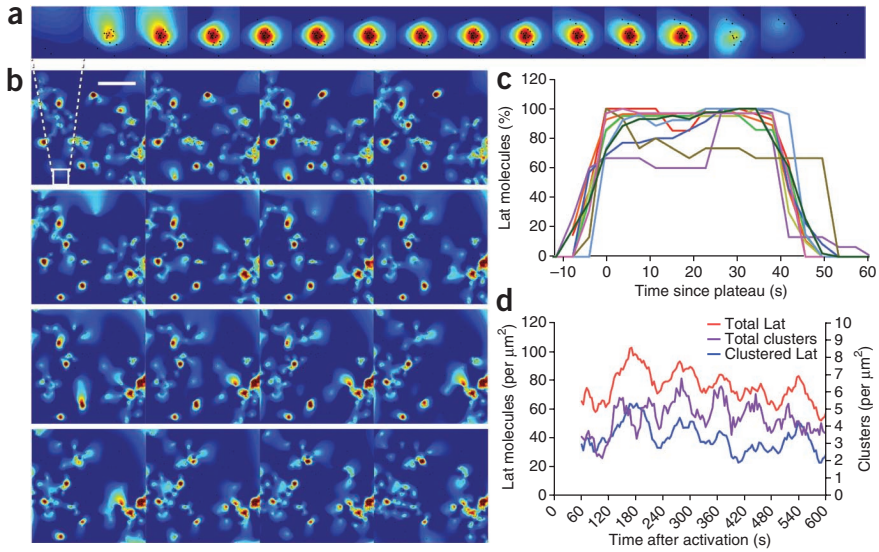

Figure 5 Live-cell PALM imaging of Lat in activated T cells. (**a**,**b**) Lifetime of a single, relatively immobile cluster of Lat (**a**) from an image sequence (at intervals of 2.9 s) of a cluster map 'movie' (**b**) of a Lat-mEos2–expressing JCaM2 cell imaged while interacting with an activating surface. Scale bar, 1 μm. (**c**) Lifetime of individual clusters of Lat in activated Lat-mEos2–expressing JCaM2 cells from the movie in **b**. (**d**) Density of total Lat or clustered Lat and number of Lat clusters over the entire plasma membrane and the 10-minute activation course in the movie in **b**. Data are representative of three experiments.

Lat clustering in live T cells

To conclusively determine whether newly recruited clusters of Lat are formed because of lateral translocation of pre-existing clusters of Lat, are recruited from an intracellular vesicular pool or are formed from Lat monomers already residing at the plasma membrane, we did live-cell PALM imaging. We combined 3,000 acquisition frames (equivalent to 47 s) into one cluster map and shifted them by 250 frames (2.9 s) to generate a cluster-map movie (**Fig. 5a**,**b** and **Supplementary Video 1**). This showed that clusters of Lat grew from small foci of Lat molecules and did not move laterally. These immobile clusters were in the size range of the 'new' TCR-induced clusters observed above (**Figs. 2d** and **3e**). The lifetime at or near the plasma membrane was 40–50 s, with clusters appearing and disappearing very quickly (**Fig. 5c**), movements reminiscent of that of vesicles docking and undocking at the membrane[28].

When viewed over the entire membrane, the total number of Lat molecules showed high correlation with the population of clustered Lat and the number of Lat clusters (**Fig. 5d**). The finding that new Lat molecules were being recruited to and driven from the membrane-proximal region in synchrony with the arrival and disappearance of Lat clusters indicated that newly recruited Lat molecules were delivered as discrete units, which lent further weight to the proposal of a vesicular process. Conversely, if Lat clustering were driven by the aggregation of small pre-existing clusters or monomeric Lat in the plasma membrane, it would be expected that the total Lat population at the membrane would remain relatively stable, whereas the population of clustered Lat molecules and Lat clusters would fluctuate. Furthermore, we identified sites in the cell membrane in which clusters of Lat repeatedly appeared and disappeared (**Supplementary Fig. 5**). In conclusion, the live-cell PALM data showed that clusters of Lat were laterally immobile and remained at or near the plasma membrane for less than a minute in activated cells.

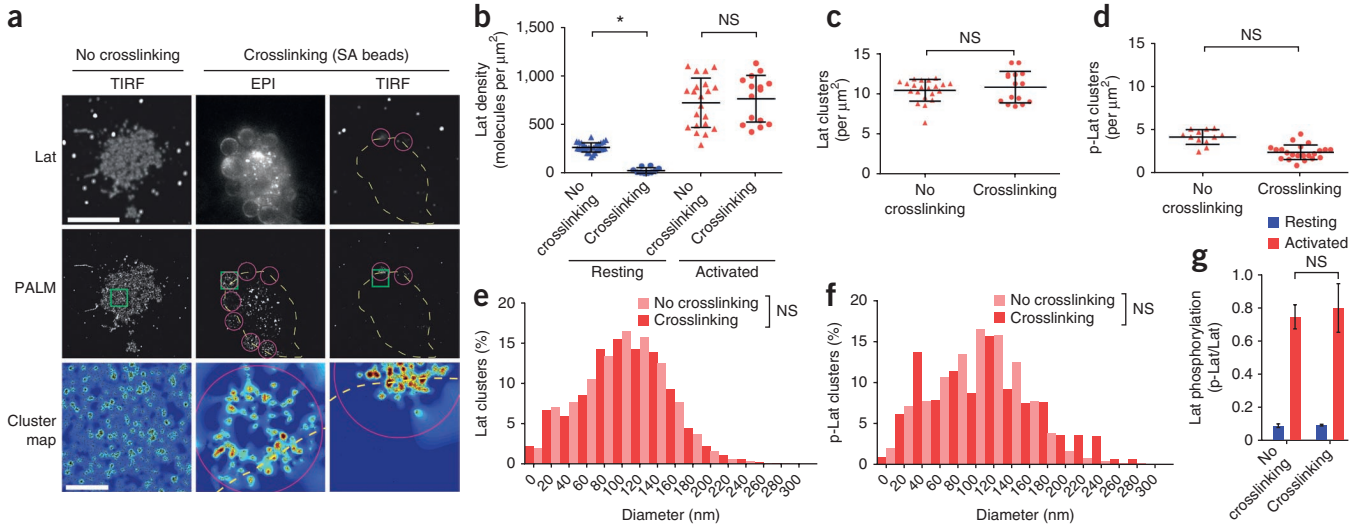

Figure 6 Crosslinking of Lat at the cell surface. (**a**) TIRF and epifluorescence (EPI) images of JCaM2 cells expressing biotinylated AP-Lat, assessed without (No crosslinking) and with (Crosslinking) incubation with streptavidin-coated beads (SA beads; purple circles); PALM images were converted to Lat cluster maps by local point-pattern analysis. Yellow dashed lines indicate cell outlines. Scale bars, 10 μm (TIRF and EPI) or 1 μm (cluster map). (**b**–**d**) Lat density in the TIRF zone in resting and activated JCaM2 cells expressing AP-Lat (**b**), and density of Lat clusters (**c**) and phosphorylated Lat clusters (**d**) in the TIRF zone in activated JCaM2 cells expressing AP-Lat, assessed before and after crosslinking of AP-Lat. $^*P < 0.0001$ (Student's *t*-test). (**e**,**f**) Distribution of sizes of clusters of Lat ($n = 15$; **e**) and phosphorylated Lat ($n = 22$; **f**) in activated JCaM2 cells, obtained by analysis of PALM image regions by local point-pattern analysis and application of a cluster threshold. (**g**) Quantification of immunoblot analysis of phosphorylated Lat and total Lat in resting and activated JCaM2 cells before and after crosslinking of AP-Lat. Data are representative of three experiments (mean and s.d. in **b**–**d**,**g**).

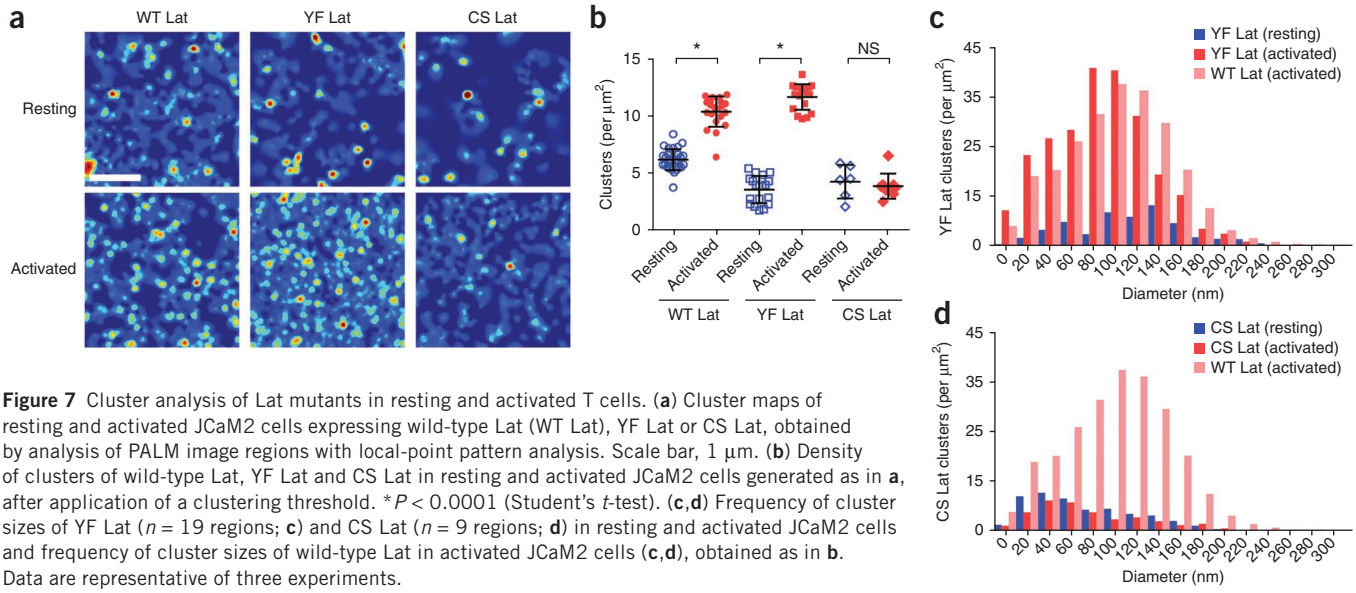

Figure 7 Cluster analysis of Lat mutants in resting and activated T cells. (**a**) Cluster maps of resting and activated JCaM2 cells expressing wild-type Lat (WT Lat), YF Lat or CS Lat, obtained by analysis of PALM image regions with local-point pattern analysis. Scale bar, 1 μm. (**b**) Density of clusters of wild-type Lat, YF Lat and CS Lat in resting and activated JCaM2 cells generated as in **a**, after application of a clustering threshold. $*P < 0.0001$ (Student's *t*-test). (**c**,**d**) Frequency of cluster sizes of YF Lat ($n = 19$ regions; **c**) and CS Lat ($n = 9$ regions; **d**) in resting and activated JCaM2 cells and frequency of cluster sizes of wild-type Lat in activated JCaM2 cells (**c**,**d**), obtained as in **b**. Data are representative of three experiments.

Crosslinking of Lat at the cell surface

Our data suggested that newly recruited Lat molecules become phosphorylated, whereas pre-existing clusters of Lat may not contribute to TCR signaling. To test this model directly, we engineered a Lat molecule with a 15–amino acid acceptor peptide on the extracellular domain (AP-Lat)[29] that could be crosslinked through the use of exogenously added streptavidin-coated beads (**Fig. 6**). The interaction between AP-Lat and beads was so efficient that non-crosslinked regions of the membrane adjacent to the glass surface (**Fig. 6a**) had a lower Lat density than that of membranes in which Lat was not crosslinked (**Fig. 6b**). The recruitment of Lat after TCR activation, however, was independent of Lat crosslinking, so the density of Lat was similar in activated T cells before and after Lat crosslinking (**Fig. 6b**). In activated T cells we found no significant difference in the degree of clustering of Lat (**Fig. 6c**) or phosphorylated Lat (**Fig. 6d**) before and after crosslinking. Further, the size distribution of clusters of Lat (**Fig. 6e**) and phosphorylated Lat (**Fig. 6f**) was also not affected by crosslinking of surface Lat. In fact, the clustering activity of AP-Lat, independent of crosslinking, mirrored that of endogenous Lat (**Fig. 3c–e**), with clusters of phosphorylated Lat appearing as distinct entities. The phosphorylation of Lat, assessed by immunoblot analysis, occurred to a similar degree in crosslinked, activated JCaM2 cells and in non-crosslinked cells (**Fig. 6g**). Hence, shifting the balance of Lat in the plasma membrane toward a more clustered configuration by crosslinking of surface Lat had no effect on the recruitment or phosphorylation of Lat. These data therefore support a model in which pre-existing clusters of Lat do not participate in early T cell signaling events.

Lat phosphorylation requires recruitment

Our data suggested that TCR ligation preconditions the membrane for vesicle recruitment and bulk activation of the Lat signaling network. An implication of this model is that recruitment of Lat precedes and is a prerequisite for phosphorylation of Lat. In contrast, the present view of the assembly of Lat signaling complexes is that the clustering and phosphorylation of Lat are part of the same process and are therefore interdependent. To assess the relationship between recruitment and phosphorylation, we used Lat mutants that either cannot be phosphorylated, because all nine tyrosine residues are substituted with phenylalanine (YF Lat)[30], or have impaired recruitment to the plasma membrane[31,32], because they do not contain the two palmitoylation sites (CS Lat)[27]. Like wild-type Lat, each Lat mutant formed clusters in resting T cells to a similar extent (**Fig. 7a**). In agreement with the predictions of our model, YF Lat was recruited as efficiently as wild-type Lat was, whereas CS Lat was not, which resulted in significantly different numbers of Lat clusters after TCR activation (**Fig. 7b**). After TCR activation, clusters of YF Lat had a size profile similar to that of clusters of wild-type Lat (**Fig. 7c**). In contrast, TCR activation had no effect on the size of clusters of CS Lat, so that cluster sizes in activated cells were very different for wild-type Lat and CS Lat (**Fig. 7d**). The lack of recruitment and clustering of CS Lat after TCR activation correlated with the lack of TCR-induced phosphorylation[33,34] (**Supplementary Fig. 6**). As CS Lat is laterally mobile[27], the lack of clustering of CS Lat provides further support for the idea that TCR-induced clusters of Lat are not preassembled or formed from Lat monomers already at the plasma membrane. In conclusion, the use of Lat mutants provided evidence that the recruitment of Lat precedes and is essential for the phosphorylation of Lat. Hence, a model has emerged in which TCR activation initiates the recruitment and subsequent phosphorylation of subsynaptic Lat-containing vesicles (**Supplementary Fig. 7**).

DISCUSSION

Here we investigated the distribution of Lat molecules at the T cell synapse by super-resolution fluorescence microscopy and quantitative cluster analysis. Lat, an integral membrane protein, is required for TCR signal transduction linking antigen recognition to downstream signaling events[13,16,17]. Lat exists in microclusters before[21] and after T cell activation[3,6,35,36]. By comparing quiescent and activated T cells, we have provided several lines of evidence that pre-existing clusters of Lat do not participate in early T cell signaling. First, although Lat exists as both monomers and clusters in resting T cells[21], we found that pre-existing clusters of Lat were not phosphorylated. Second, clusters of phosphorylated Lat and non-phosphorylated clusters were two distinct entities in activated T cells. Third, TCR activation recruited Lat molecules to the activation site but this recruitment did not occur at the expense of the pre-existing clusters of Lat. Finally, clusters of Lat at the TCR activation sites were laterally immobile and

were not assembled from monomeric Lat molecules. Instead, clusters of Lat had a short, sub-minute lifetime consistent with the docking of membrane-proximal vesicles to the plasma membrane[37,38]. We therefore propose a model in which TCR ligation conditions the membrane for the recruitment and phosphorylation of Lat vesicles for *en masse* activation of the Lat signaling network (signalosome)[39].

Lat complexes at the plasma membrane are thought to be the result of protein-protein interactions[27,37]. Because of its dual palmitoylation[33], Lat may also be associated with lipid rafts in T cells[40]. Raft-like membrane structures have been observed in activated T cells in the plasma membrane and subsynaptic vesicles[4,5]. Our data suggest that the clustering of Lat in the membrane is an intrinsic property of the protein itself, rather than being influenced by the physical condition and biochemical composition of the membrane. We observed that clustering efficiency was similar in nonactivated and activated regions of the same cell, whereas the biophysical and biochemical properties of these sites are different[4,41]. TCR triggering resulted in a considerable increase in Lat molecules at the cell surface, which confirmed the results of biochemical studies[42,43]. However, our data largely exclude the hypothesis that TCR-induced clusters of Lat are formed by the lateral recruitment of Lat monomers or pre-existing clusters. Furthermore, phosphorylation of Lat did not correlate with the clustering of Lat, and only a subpopulation of Lat clusters contained phosphorylated Lat. Hence, discrete Lat islands[21] or Lat microdomains[11] are formed via protein-protein interactions (and not lipid rafts[27]) in the plasma membrane but probably do not contribute to early TCR signaling events.

It has been shown that clusters of receptors and clusters of Lat remain juxtaposed but separate entities[21,44], which raises the question of how Lat is phosphorylated and participates in TCR signaling. Our single-molecule imaging approach has provided evidence that the recruitment of Lat to TCR-activation sites occurs as the docking of vesicles to the plasma membrane. The molecular photon count suggested that clustered Lat molecules translocate *en masse* to the cell surface; clusters of Lat appeared rapidly and as discrete quanta, some at predefined sites, and had a short lifetime. This model is supported by published reports of Lat in intracellular vesicles that contain markers of recycling and late endosomes[37,38] and whose dynamics are governed by the architecture of the TCR lattice[37]. Lat phosphorylation takes place when vesicular Lat transiently interacts with clusters of the adaptor SLP-76 at the cell surface[37]. Hence, TCR activation preconditions the membrane for the recruitment and phosphorylation of Lat, which enables 'bulk' activation of signaling cascades. This is distinct from a molecular assembly of signaling complexes that takes place solely within the lateral organization of the plasma membrane and in which assembly and phosphorylation are interlinked processes. Our data cannot be reconciled with such a molecular assembly model. Shifting the balance of Lat in the plasma membrane toward a more clustered configuration had no effect on the recruitment and phosphorylation of Lat. A Lat signaling mutant that cannot be phosphorylated demonstrated that recruitment was independent of phosphorylation. A transport mutant lacking the two palmitoylation sites showed that recruitment was necessary for the clustering and phosphorylation of Lat. Our data have therefore provided evidence that pre-existing clusters of Lat do not participate in early T cell signaling events and that recruitment of Lat from an intracellular vesicular pool precedes and is essential for phosphorylation of Lat.

Preconditioning of the T cell membrane for bulk activation of TCR signaling probably requires the establishment of protein networks in the membrane[37], including the recruitment and activation of kinases[12], as well as the restructuring of cortical actin[7], to facilitate the docking of vesicles at the plasma membrane. One implication of a vesicular signaling model is that signaling processes are not hierarchical but are interdependent, as shown before for Zap70 (ref. 45). It also attributes a greater regulatory role to endocytic compartments in the control of TCR signaling[28,46]. Hence, the lymphoproliferative disorders observed in mice with Lat signaling mutants[39,47] may be caused not just by impaired interactions with Lat binding partners but also by imbalances in signaling regulation due to alterations in Lat trafficking[38]. In this context, we note that intracellular trafficking pathways, rather than the rate of internalization, control the ligand-induced down-modulation of the TCR[48]. Advances in fluorescence microscopy may aid in pinpointing the location of TCR signaling complexes and delineate membrane-associated events from vesicular components for elucidation of the regulation of T cell signaling.

METHODS

Methods and any associated references are available in the online version of the paper at http://www.nature.com/natureimmunology/.

Note: Supplementary information is available on the Nature Immunology website.

ACKNOWLEDGMENTS

Supported by the National Health and Medical Research Council of Australia (D.J.W., J.J.G. and K.G.), the Australian Research Council (D.M.O., J.J.G. and K.G.) and Human Frontier Science Program (K.G.).

AUTHOR CONTRIBUTIONS

D.J.W., molecular biology, PALM, crosslinking experiments and analysis, and manuscript preparation; D.M.O., conceptualization and PALM-STORM analysis; J.R., STORM experiments and analysis; A.M., PALM experiments and analysis of surface-patterning experiments; M.W., surface-patterning experiments; J.J.G., conceptualization of surface patterning; and K.G., conceptualization and manuscript preparation.

COMPETING FINANCIAL INTERESTS

The authors declare no competing financial interests.

Published online at http://www.nature.com/natureimmunology/.
Reprints and permissions information is available online at http://www.nature.com/reprints/index.html

1. van der Merwe, P.A. & Davis, S.J. Immunology. The immunological synapse—a multitasking system. *Science* **295**, 1479–1480 (2002).
2. Varma, R., Campi, G., Yokosuka, T., Saito, T. & Dustin, M.L. T cell receptor-proximal signals are sustained in peripheral microclusters and terminated in the central supramolecular activation cluster. *Immunity* **25**, 117–127 (2006).
3. Yokosuka, T. *et al.* Newly generated T cell receptor microclusters initiate and sustain T cell activation by recruitment of Zap70 and SLP-76. *Nat. Immunol.* **6**, 1253–1262 (2005).
4. Gaus, K., Chklovskaia, E., Fazekas de St Groth, B., Jessup, W. & Harder, T. Condensation of the plasma membrane at the site of T lymphocyte activation. *J. Cell Biol.* **171**, 121–131 (2005).
5. Owen, D.M. *et al.* High plasma membrane lipid order imaged at the immunological synapse periphery in live T cells. *Mol. Membr. Biol.* **27**, 178–189 (2010).
6. Campi, G., Varma, R. & Dustin, M.L. Actin and agonist MHC-peptide complex-dependent T cell receptor microclusters as scaffolds for signaling. *J. Exp. Med.* **202**, 1031–1036 (2005).
7. Kaizuka, Y., Douglass, A.D., Varma, R., Dustin, M.L. & Vale, R.D. Mechanisms for segregating T cell receptor and adhesion molecules during immunological synapse formation in Jurkat T cells. *Proc. Natl. Acad. Sci. USA* **104**, 20296–20301 (2007).
8. Monks, C.R., Freiberg, B.A., Kupfer, H., Sciaky, N. & Kupfer, A. Three-dimensional segregation of supramolecular activation clusters in T cells. *Nature* **395**, 82–86 (1998).
9. Grakoui, A. *et al.* The immunological synapse: a molecular machine controlling T cell activation. *Science* **285**, 221–227 (1999).
10. Samelson, L.E. & Klausner, R.D. Tyrosine kinases and tyrosine-based activation motifs. Current research on activation via the T cell antigen receptor. *J. Biol. Chem.* **267**, 24913–24916 (1992).
11. Weiss, A. & Littman, D.R. Signal transduction by lymphocyte antigen receptors. *Cell* **76**, 263–274 (1994).
12. Blanchard, N., Di Bartolo, V. & Hivroz, C. In the immune synapse, ZAP-70 controls T cell polarization and recruitment of signaling proteins but not formation of the synaptic pattern. *Immunity* **17**, 389–399 (2002).

13. Finco, T.S., Kadlecek, T., Zhang, W., Samelson, L.E. & Weiss, A. LAT is required for TCR-mediated activation of PLCγ1 and the Ras pathway. *Immunity* **9**, 617–626 (1998).
14. Zhang, W., Irvin, B.J., Trible, R.P., Abraham, R.T. & Samelson, L.E. Functional analysis of LAT in TCR-mediated signaling pathways using a LAT-deficient Jurkat cell line. *Int. Immunol.* **11**, 943–950 (1999).
15. Zhang, W. *et al.* Essential role of LAT in T cell development. *Immunity* **10**, 323–332 (1999).
16. Aguado, E., Martinez-Florensa, M. & Aparicio, P. Activation of T lymphocytes and the role of the adapter LAT. *Transpl. Immunol.* **17**, 23–26 (2006).
17. Shen, S. *et al.* The importance of LAT in the activation, homeostasis, and regulatory function of T cells. *J. Biol. Chem.* **285**, 35393–35405 (2010).
18. Ilani, T., Vasiliver-Shamis, G., Vardhana, S., Bretscher, A. & Dustin, M.L. T cell antigen receptor signaling and immunological synapse stability require myosin IIA. *Nat. Immunol.* **10**, 531–539 (2009).
19. Lee, K.H. *et al.* T cell receptor signaling precedes immunological synapse formation. *Science* **295**, 1539–1542 (2002).
20. Lee, K.H. *et al.* The immunological synapse balances T cell receptor signaling and degradation. *Science* **302**, 1218–1222 (2003).
21. Lillemeier, B.F. *et al.* TCR and Lat are expressed on separate protein islands on T cell membranes and concatenate during activation. *Nat. Immunol.* **11**, 90–96 (2010).
22. Betzig, E. *et al.* Imaging intracellular fluorescent proteins at nanometer resolution. *Science* **313**, 1642–1645 (2006).
23. Hess, S.T., Girirajan, T.P. & Mason, M.D. Ultra-high resolution imaging by fluorescence photoactivation localization microscopy. *Biophys. J.* **91**, 4258–4272 (2006).
24. Rust, M.J., Bates, M. & Zhuang, X. Sub-diffraction-limit imaging by stochastic optical reconstruction microscopy (STORM). *Nat. Methods* **3**, 793–795 (2006).
25. Heilemann, M. *et al.* Subdiffraction-resolution fluorescence imaging with conventional fluorescent probes. *Angew. Chem. Int. Edn Engl.* **47**, 6172–6176 (2008).
26. Mattheyses, A.L. & Axelrod, D. Direct measurement of the evanescent field profile produced by objective-based total internal reflection fluorescence. *J. Biomed. Opt.* **11**, 014006 (2006).
27. Douglass, A.D. & Vale, R.D. Single-molecule microscopy reveals plasma membrane microdomains created by protein-protein networks that exclude or trap signaling molecules in T cells. *Cell* **121**, 937–950 (2005).
28. Scita, G. & Di Fiore, P.P. The endocytic matrix. *Nature* **463**, 464–473 (2010).
29. Howarth, M., Takao, K., Hayashi, Y. & Ting, A.Y. Targeting quantum dots to surface proteins in living cells with biotin ligase. *Proc. Natl. Acad. Sci. USA* **102**, 7583–7588 (2005).
30. Hartgroves, L.C. *et al.* Synergistic assembly of linker for activation of T cells signaling protein complexes in T cell plasma membrane domains. *J. Biol. Chem.* **278**, 20389–20394 (2003).
31. Tanimura, N., Saitoh, S., Kawano, S., Kosugi, A. & Miyake, K. Palmitoylation of LAT contributes to its subcellular localization and stability. *Biochem. Biophys. Res. Commun.* **341**, 1177–1183 (2006).
32. Hundt, M. *et al.* Palmitoylation-dependent plasma membrane transport but lipid raft-independent signaling by linker for activation of T cells. *J. Immunol.* **183**, 1685–1694 (2009).
33. Zhang, W., Trible, R.P. & Samelson, L.E. LAT palmitoylation: its essential role in membrane microdomain targeting and tyrosine phosphorylation during T cell activation. *Immunity* **9**, 239–246 (1998).
34. Lin, J., Weiss, A. & Finco, T.S. Localization of LAT in glycolipid-enriched microdomains is required for T cell activation. *J. Biol. Chem.* **274**, 28861–28864 (1999).
35. Montoya, M.C. *et al.* Role of ICAM-3 in the initial interaction of T lymphocytes and APCs. *Nat. Immunol.* **3**, 159–168 (2002).
36. Bunnell, S.C. *et al.* T cell receptor ligation induces the formation of dynamically regulated signaling assemblies. *J. Cell Biol.* **158**, 1263–1275 (2002).
37. Purbhoo, M. *et al.* Dynamics of subsynaptic vesicles and surface microclusters at the immunological synapse. *Sci. Signal.* **3**, ra36–ra36 (2010).
38. Bonello, G. *et al.* Dynamic recruitment of the adaptor protein LAT: LAT exists in two distinct intracellular pools and controls its own recruitment. *J. Cell Sci.* **117**, 1009–1016 (2004).
39. Malissen, B., Aguado, E. & Malissen, M. Role of the LAT adaptor in T-cell development and Th2 differentiation. *Adv. Immunol.* **87**, 1–25 (2005).
40. Tanimura, N. *et al.* Dynamic changes in the mobility of LAT in aggregated lipid rafts upon T cell activation. *J. Cell Biol.* **160**, 125–135 (2003).
41. Zech, T. *et al.* Accumulation of raft lipids in T-cell plasma membrane domains engaged in TCR signalling. *EMBO J.* **28**, 466–476 (2009).
42. Harder, T. & Kuhn, M. Selective accumulation of raft-associated membrane protein LAT in T cell receptor signaling assemblies. *J. Cell Biol.* **151**, 199–208 (2000).
43. Rentero, C. *et al.* Functional implications of plasma membrane condensation for T cell activation. *PLoS ONE* **3**, e2262 (2008).
44. Wilson, B.S., Pfeiffer, J.R., Surviladze, Z., Gaudet, E.A. & Oliver, J.M. High resolution mapping of mast cell membranes reveals primary and secondary domains of FcεRI and LAT. *J. Cell Biol.* **154**, 645–658 (2001).
45. Liu, H., Purbhoo, M.A., Davis, D.M. & Rudd, C.E. SH2 domain containing leukocyte phosphoprotein of 76-kDa (SLP-76) feedback regulation of ZAP-70 microclustering. *Proc. Natl. Acad. Sci. USA* **107**, 10166–10171 (2010).
46. Barr, V.A. *et al.* T-cell antigen receptor-induced signaling complexes: internalization via a cholesterol-dependent endocytic pathway. *Traffic* **7**, 1143–1162 (2006).
47. Mingueneau, M. *et al.* Loss of the LAT adaptor converts antigen-responsive T cells into pathogenic effectors that function independently of the T cell receptor. *Immunity* **31**, 197–208 (2009).
48. Liu, H., Rhodes, M., Wiest, D.L. & Vignali, D.A. On the dynamics of TCR:CD3 complex cell surface expression and downmodulation. *Immunity* **13**, 665–675 (2000).

ONLINE METHODS

Cells and surfaces. JCaM2 cells and the wild-type Jurkat cell line E6.1 were cultured in RPMI medium (Gibco) supplemented with 10% (vol/vol) FCS and were transfected by electroporation (NEON; Invitrogen). Primary mouse T cells were isolated from the spleens of C57BL/6 mice (in accordance with the Animal Care and Ethics Committee of the University of New South Wales) by negative magnetic separation (Miltenyi Biotec); 85.7% ± 1.6% of cells were $CD3^+$, as determined by flow cytometry. For activation of cells expressing wild-type Lat, YF Lat and CS Lat fused to mEos2 on glass coverslips coated with anti-CD3 (16-0037; eBioscience) and anti-CD28 (16-0289; eBioscience), cells were allowed to settle on the activating surface for 10 min at 37 °C. Antibody was adsorbed onto clean glass coverslips by incubation for at least 1 h at 37 °C with antibody solution (10 µg/ml). Cells were fixed with 4% (wt/vol) paraformaldehyde in PBS and were made permeable for immunostaining with lysolecithin (100 µg/ml; L5254; Sigma). Resting JCaM2 cells were first fixed in suspension and then were centrifuged on a nonactivating bare coverglass surface (control experiments, **Supplementary Fig. 3**).

Rabbit polyclonal anti-Lat (9166; Cell Signaling) or antibody to Lat phosphorylated at Tyr191 (44-228; Invitrogen) was used for immunostaining. Antibodies were probed with DyLight 649–conjugated secondary goat antibody to rabbit $F(ab')_2$ fragment (111-495-047; Jackson ImmunoResearch Laboratories). For dSTORM imaging, the following oxygen-scavenging PBS solution was used: 25 mM HEPES, pH 8.0, 25 mM glucose, 5% (vol/vol) glycerol, glucose oxidase (0.05 mg/ml) and horseradish peroxidase (0.025 mg/ml), supplemented with 75 mM cysteamine (all from Sigma).

Micro-patterned activation surfaces were produced with a Nano eNabler (BioForce) by deposition of spots of anti-CD3 and anti-CD28 4 µm in diameter onto glass coverslips in a grid with spot separation of 14 µm (center to center). Before deposition of antibody, coverslips were cleaned for 30 min in 'piranha solution' (H_2O_2 and H_2SO_4 at a ratio of 3:7), were modified for 48 h with a self-assembled monolayer of octadecyltrichlorosilane (Sigma) and were coated for 5 min with poly-L-lysine (0.1 mg/ml; Sigma).

Escherichia coli biotin ligase (BirA) was expressed and purified as described[49]. Lat was biotinylated for 30 min at 37 °C on transfected cells in suspension with 0.3 µM BirA, 1 mM ATP and 10 µM biotin. Streptavidin-conjugated polystyrene beads (SVP-30-5; Spherotech) were incubated for 10 min at 37 °C with biotinylated cells in suspension. Biotinylated cells with and without crosslinkage were imaged or lysed (for immunoblot analysis) as resting and activated cells as described above.

Imaging. PALM and dSTORM images were acquired on a TIRF microscope (ELYRA; Zeiss) with a 100× oil-immersion objective with a numerical aperture of 1.46. For mEos2, photoconversion was achieved with 8 µW of 405-nm laser radiation, and 'red-converted' mEos2 was imaged with 12 mW of 561-nm light. For dSTORM with DyLight 649, imaging was done with 15 mW of 633-nm laser illumination and conversion from the dark state with 0.1–1 mW of 488 nm. For PALM and dSTORM, 1.5×10^5 to 2×10^5 raw images were acquired per sample with a cooled, electron-multiplying charge-coupled device camera (iXon DU-897D; Andor) with an exposure time of 30 ms. For live-cell PALM of mEos2, the imaging laser was increased to 18 mW and the camera exposure was decreased to 5 ms. Recorded images were analyzed with Zeiss ZEN software (**Supplementary Methods**). Drifts were corrected to surface-immobilized 100-nm colloidal gold beads (BBInternational) on each sample.

Data analysis and statistics. Two-dimensional molecular coordinates were cropped into nonoverlapping regions 3 µm × 3 µm in size, and events with a localization precision worse than 50 nm were discarded. Ripley's K-function analysis and quantitative cluster maps were generated as described[50]. Clustering threshold values were set so that $L(r) > 78$ with the radial scale $r = 50$ nm, corresponding to approximately 30% of each region's cluster-map maximum. Circularity was measured with ImageJ image-processing software (US National Institutes of Health). Additional details are in the **Supplementary Methods** and **Supplementary Figures 1** and **2**. For live-cell PALM, 3×10^3 raw images were used for the construction of each cluster map. The 3,000-frame window was then shifted by 250 frames for construction of the next cluster map.

The statistical significance of the means of two data sets was assessed by Student's *t*-test; multiple comparisons were made with one-way analysis of variance and Bonferroni post-testing; and nonlinear curve fitting was used to fit normalized histograms to a single Gaussian distribution (Prism, GraphPad Software).

Immunoblot analysis. Whole-cell lysates were prepared in radioimmunoprecipitation buffer containing 150 mM NaCl, 50 mM Tris-HCl, pH 7.4, 1% (vol/vol) NonidetP-40, 0.25% (wt/vol) sodium deoxycholate and supplemented with protease and phosphatase inhibitors (cOmplete ULTRA and PhosSTOP; Roche). Equal amounts of protein were resolved by denaturing SDS-PAGE and were detected by immunoblot analysis with anti-Lat (9166; Cell Signaling) or antibody to Lat phosphorylated at Tyr191 (44-228; Invitrogen).

49. Chen, I., Howarth, M., Lin, W. & Ting, A.Y. Site-specific labeling of cell surface proteins with biophysical probes using biotin ligase. *Nat. Methods* **2**, 99–104 (2005).
50. Owen, D.M. *et al.* PALM imaging and cluster analysis of protein heterogeneity at the cell surface. *J Biophotonics* **3**, 446–454 (2010).

Pre-existing clusters of the adaptor Lat do not participate in early T cell signaling events

David J. Williamson[1,3], Dylan M. Owen[1,3], Jérémie Rossy[1,3], Astrid Magenau[1], Matthias Wehrmann[2], J. Justin Gooding[2] and Katharina Gaus[1]

[3]These authors contributed equally

[1]Centre for Vascular Research, University of New South Wales, Sydney, Australia
[2]School of Chemistry and the Australian Centre for Nanomedicine, University of New South Wales, Sydney, Australia

[3]These authors contributed equally

Correspondence should be addressed to:
Katharina Gaus, Centre for Vascular Research, University of New South Wales, Sydney, 2052, NSW, Australia. Tel.: +61 2 9385 1377; Fax: +61 2 9385 1389. Email: k.gaus@unsw.edu.au

SUPPLEMENTARY MATERIAL

Generation of PALM and dSTORM images

To obtain the x-y coordinates of molecules for a PALM or dSTORM image, a fluorescence intensity image captured by a camera (**Supplementary Fig. 1a**) was analyzed with an algorithm that identifies the centre of the point-spread-function (PSF) of each molecule as previously described[1] (Zen 6.3, Carl Zeiss Microimaging GmbH). For the algorithms to work optimally, the input data was required to have a high signal-to-noise ratio (SNR). The SNR was enhanced by total internal reflectance fluorescence (TIRF) excitation, which limits the imaging to molecules that are within ≈150 nm of the glass surface thus removing out-of-focus light. To calculate the centre of observed PSFs a Gaussian mask was used, which represents a good compromise between speed and precision. The Gaussian mask method employs a centre-of-gravity calculation weighted by a smooth Gaussian curve. Thompson *et al.* laid out the theory for this analysis method that allows the precision of localization (Δx) for a 2-D PSF to be determined[1]. In order to calculate the localization precision, the number of collected photons (N), the width of the PSF (s), and the background variance (b) must be known for each event. These parameters are illustrated in **Supplementary Figure 1b**.

All acquisition frames were corrected for any mechanical or thermal drift during the image acquisition, chromatic aberrations and frame shifts (which can occur by changing emission filters, for example). This was achieved by placing immobile fiducials (100 nm gold beads) in the sample and correcting the frames during the image processing.

The first step in the data analysis post acquisition is to detect the single molecule events. Images were first Gaussian and Laplace filtered. The mean (M) and standard deviation (S) of

Nature Immunology doi:10.1038/ni.2049

the resulting image were then calculated. The criteria for single molecule detection of a spot of intensity (I) is then given as when I-M > S*SNR, where SNR = 5. **Supplementary Figure 1c** shows the number of events detected and the median localization precision value for all events in a representative image processed with different SNR ratios. The data illustrate that there was a non-linear change in the number of detected molecules and their precision at SNR values between 3 and 4. Beyond a SNR of 6, there was little improvement in precision; below 4 a large numbers of background events were counted as single molecules. Therefore, a SNR of 5 was appropriate and was used throughout. For mEos2, a PSF width (1σ) of 86 nm was used. A value of 98 nm was used for DyLight649. While mEos2 and dSTORM probes (DyLight649) have been shown to blink on multiple timescales[2] this blinking would not be expected to change depending on the activation state of cells and therefore multiple activations are unlikely to affect ratiometric measurements. Nevertheless, in dSTORM data where multiple localizations from the same molecule are expected to be most severe, events whose localizations appear in the same area within 50 frames (off-gap) were summed and counted as one molecule. To justify this threshold, we plotted the histogram of the number of molecules with frames missing in their detected fluorescence signal for a representative experiment (**Supplementary Fig. 1d**). Events with missing frames are potentially re-excited molecules. Although fluorescence blinking can in principle occur on various time scales, it appeared that most reinitiated photo-activation occurred within the first 15 frames or 0.45 seconds after the initial excitation. We therefore included off-gap=50 frames as an additional threshold parameter. The off-gap defines the time period (in frames) in which fluorescent events that localize to the same area were counted as one molecule. **Supplementary Figure 1e** shows the effect of increasing the off-gap on the number of molecules. Off gap times greater than 50 frames did not significantly reduce the number of detected molecules suggesting that our molecule selection with these threshold parameters (SNR = 5; off-gap = 50 frames) was highly unlikely to include background fluorescence and re-excited molecules. It should be noted that the counting of molecules is only accurate in the context of these acquisition and threshold parameters, which were kept constant throughout the manuscript.

Once the events were detected, the data was exported as a table containing information on the x-y coordinates of each molecule, the frame number in which the event was first detected, the photon count of the molecule, its associated background value and localization precision.

These data was used to construct a 2-D spatial point pattern of the molecular distribution. Ripley's K-function was then calculated using SpPack[3] as:

$$\text{For } i \neq j$$

$$K(r) = A\sum_{i=1}^{n}\sum_{j=1}^{n}\left(\frac{\delta_{ij}}{n^2}\right) \text{ where } \delta_{ij} = 1 \; if \; \delta_{ij} < r, \text{otherwise } 0 \qquad \text{(Equation 1)}$$

Nature Immunology doi:10.1038/ni.2049

where A is the area of the analyzed region (here 3 x 3 μm), n is the number of points, r is the spatial scale (radius) for the K-function calculation and δ_{ij} is the distance between points i and j. This counts the number of molecules encircled by concentric rings centered on each molecule, normalized to the average molecular density of the entire region. This function was then linearized to generate the L-function according to:

$$L(r) = \sqrt{K(r)/\pi} \qquad \text{(Equation 2)}$$

such that L(r) scales linearly with radius. For completely spatially random distributions of molecules, L(r)=r. We hence plotted L(r)-r (sometimes termed the H-function) against r such that a random distribution has L(r)-r = zero for all r. Therefore, for length scales at which the distribution is more clustered than a random distribution, L(r)-r was positive, whereas L(r)-r was negative if the points are less clustered than for random events. Points at the edge of the distribution region were weighted to negate edge-related effects. Confidence intervals were generated by simulating 100 spatially random distributions with the same average molecular density as the data regions.

Values of L(r) generated for each point (ignoring the j-sum in Equation 1, (Getis and Franklin's method) at a value of r=50 nm (L(50)) were then calculated. These were used to produce a map of clustering by interpolating a surface plot with L(50) as the z-axis (pseudo-color scale). Spatial interpolation was performed on a grid of resolution 10 nm using MATLAB interpolation 'v4' (MATLAB, The Mathworks Inc., Natick, MA) to generate a 2-dimensional cluster 'heat' map.

Cluster maps were thresholded to produce binary cluster maps. Here, areas of the interpolated map with L(50)>78 were defined as clusters. Similarly, individual molecular localizations with L(50)>78 were defined as being in clusters and those ≤78 as being outside clusters. In typical data sets, this threshold was ≈30% of the peak value in any region and was sufficient to exclude cluster detection in spatially random simulated data. From the binary map, the number of clusters, cluster size, fraction of the map covered by clusters and the shape etc. were extracted and analyzed. This method was shown to be effective at extracting these clustering characteristics for PALM data, dSTORM data and simulated data[4].

As there is typically a distribution of localization precision, photon count and background values, we cropped, or thresholded, the data before image analysis to generate an image with definable resolution. This presented an additional complication in the choice of parameters to threshold. Two different cases may be considered: cropping by precision directly (here for example at Δx<50 nm), or cropping by the photon counts (e.g. N=100-2000) and background level (e.g. b<30), which go into calculating the precision. In this example, the values of these parameters selected in the crop are shown in the histograms (**Supplementary Fig. 2a**). It might be expected that these two operations would produce the same result. However, this was not the case. This can be immediately seen in the plots of

Nature Immunology doi:10.1038/ni.2049

photon count *versus* precision (**Supplementary Fig. 2b-d**). For the two different cropping methods, different events were included in further analysis or excluded from the PALM/dSTORM image. This is illustrated for an example data set (**Supplementary Fig. 2e**), for which quantitative cluster maps of a 3 µm x 3 µm area were constructed (**Supplementary Fig. 2f-h**): **Supplementary Fig. 2f** was constructed from the raw, non-thresholded data, **Supplementary Fig. 2g** was thresholded by precision at a value of 50 nm, and **Supplementary Fig. 2h** was thresholded by photon count (N=100-2000 photons/molecule) and background variance (b<30). The degree of clustering illustrated the requirement to threshold as Lat microclusters that were easily visible in either thresholded (**Supplementary Fig. 2g-h**) data sets were not apparent in the non-thresholded data (**Supplementary Fig. 2f**) due to mis-localized molecules. In addition, cluster maps generated from data that were thresholded by photon-count/background or precision value alone were not identical. Some clusters (highlighted) appeared in the precision-thresholded map but not in the photon-count/background-thresholded map. Molecules in these areas had low photon counts, but maintained relatively high precision. We attributed these data to molecules relatively high in the evanescent field as they also displayed comparatively low background. To avoid that vesicles were removed from the cluster map, we applied a precision threshold of <50 nm only to our data throughout this study.

Plasmids

Mammalian expression constructs encoding full-length wildtype human Lat variant 2 and the non-signaling YF Lat mutant were a gift from Thomas Harder (University of Oxford). The palmitoylation deficient CS Lat construct was a kind gift from Ronald Vale (University of California, San Francisco). mEos2 expression constructs were a gift from Jörg Wiedenmann (University of Southampton). Biotin ligase bacterial expression constructs and acceptor peptide sequences were a gift from Alice Ting (Massachusetts Institute of Technology).

Sample preparation

Throughout the manuscript, we compared Lat clustering in resting T cells that were fixed in suspension and adhered onto uncoated coverslips by centrifugation (2 min, 145 g) to T cells activated on coverslips coated with anti-CD3 and anti-CD28 followed by fixation. No phosphorylation of CD3ζ or Lat was detected in resting cells by TIRF microscopy. To ensure that the sample preparation did not affect the quantification of Lat clustering behavior, we performed a series of control experiments by comparing the size distribution of Lat clusters under various sample preparation conditions.

First, we compared the distribution of Lat cluster sizes, acquired by PALM, in resting cells that were fixed in solution and then spun onto bare surfaces with resting cells that were allowed to settle onto non-activating IgG-coated glass and then fixed as adherent cells. No significant difference between the size distribution histograms was observed (p>0.05, **Supplementary Fig. 3a**). This shows that the adherence by centrifugation of fixed, resting cells did not artificially alter Lat clustering behavior. Similarly for activated cells, we

Nature Immunology doi:10.1038/ni.2049

compared the distribution of Lat cluster sizes in cells activated by soluble antibodies (anti-CD3 and anti-CD28), fixed in suspension and spun onto bare glass with Lat cluster sizes in cells activated by antibody-coated glass coverslips. Again, no significant difference ($p>0.05$, **Supplementary Fig. 3b**) was observed. It was noted that while total Lat density was higher in non-activated cells on IgG-coated glass (715.1 ± 101.9 Lat molecules/μm^2) than in non-activated cells fixed in suspension (267.9 ± 47.49 Lat molecules/μm^2), we found a lower Lat density in cells activated with adherent antibodies (723.5 ± 251.8 Lat molecules/μm^2) than in cells activated with soluble antibodies and fixed in suspension (1046 ± 92.67 Lat molecules/μm^2). This suggests that our measurements were not affected by the sample preparation (fixation in suspension followed by centrifugation *versus* adherence onto antibody-coated glass followed by fixation) and that the association of the cells with the glass surface is likely to be similar in both sample architectures. Rather, the data suggest that adherence, even onto non-activating antibodies results in a partial T cell activation, possibly due to adherence-induced shape change and polarization. We therefore used fixation in suspension as the sample preparation for resting cells and the more physiological relevant stimulation with anti-CD3/CD28-coated glass for T cell activation. In conclusion, these data indicate that differences in Lat clustering observed between resting and activated T cells was not due to different methods of sample preparation.

We next checked for differences in Lat clustering caused by either fixation and permeabilization as some membrane proteins were shown to remain mobile after PFA fixation[5]. Comparing T cells fixed with 4% PFA for 30 min or fixed in 0.1% cold methanol for 1 min, no differences in Lat cluster sizes were observed ($p>0.05$, **Supplementary Fig. 3c**) suggesting that PFA fixation did not induce Lat clustering by incomplete fixation. Finally, we compared Lat cluster sizes in activated cells before and after irreversible permeabilization with lysolecithin (100 µg/mL) as this method was used for immunostaining for dSTORM acquisitions. No differences in Lat cluster sizes were observed between permeabilized and non-permeabilized cells ($p>0.05$, **Supplementary Fig. 3d**). The data demonstrate that fixation and permeabilization had no effect on Lat clustering.

References

1. Thompson, R.E., Larson, D.R. & Webb, W.W. Precise nanometer localization analysis for individual fluorescent probes. *Biophys J* **82**, 2775-2783 (2002).
2. Annibale, P., Scarselli, M., Kodiyan, A. & Radenovic, A. Photoactivatable Fluorescent Protein mEos2 Displays Repeated Photoactivation after a Long-Lived Dark State in the Red Photoconverted Form. *Journal of Physical Chemistry Letters* **1**, 1506-1510 (2010).
3. Perry, G.L.W. SpPack: spatial point pattern analysis in Excel using Visual Basic for Applications (VBA). *Environmental Modelling & Software* **19**, 559-569 (2004).
4. Owen, D.M. *et al.* PALM imaging and cluster analysis of protein heterogeneity at the cell surface. *Journal of Biophotonics* **3**, 446-454 (2010).
5. Tanaka, K.A.K. *et al.* Membrane molecules mobile even after chemical fixation. *Nat. Meth.* **7**, 865-866 (2010).

Nature Immunology doi:10.1038/ni.2049

6. Bonello, G. *et al.* Dynamic recruitment of the adaptor protein LAT: LAT exists in two distinct intracellular pools and controls its own recruitment. *J Cell Sci* **117**, 1009-1016 (2004).
7. Lillemeier, B.F. *et al.* TCR and Lat are expressed on separate protein islands on T cell membranes and concatenate during activation. *Nat Immunol* **11**, 90-96 (2010).
8. Purbhoo, M. *et al.* Dynamics of Subsynaptic Vesicles and Surface Microclusters at the Immunological Synapse. *Science Signaling* **3**, ra36-ra36 (2010).

Nature Immunology doi:10.1038/ni.2049

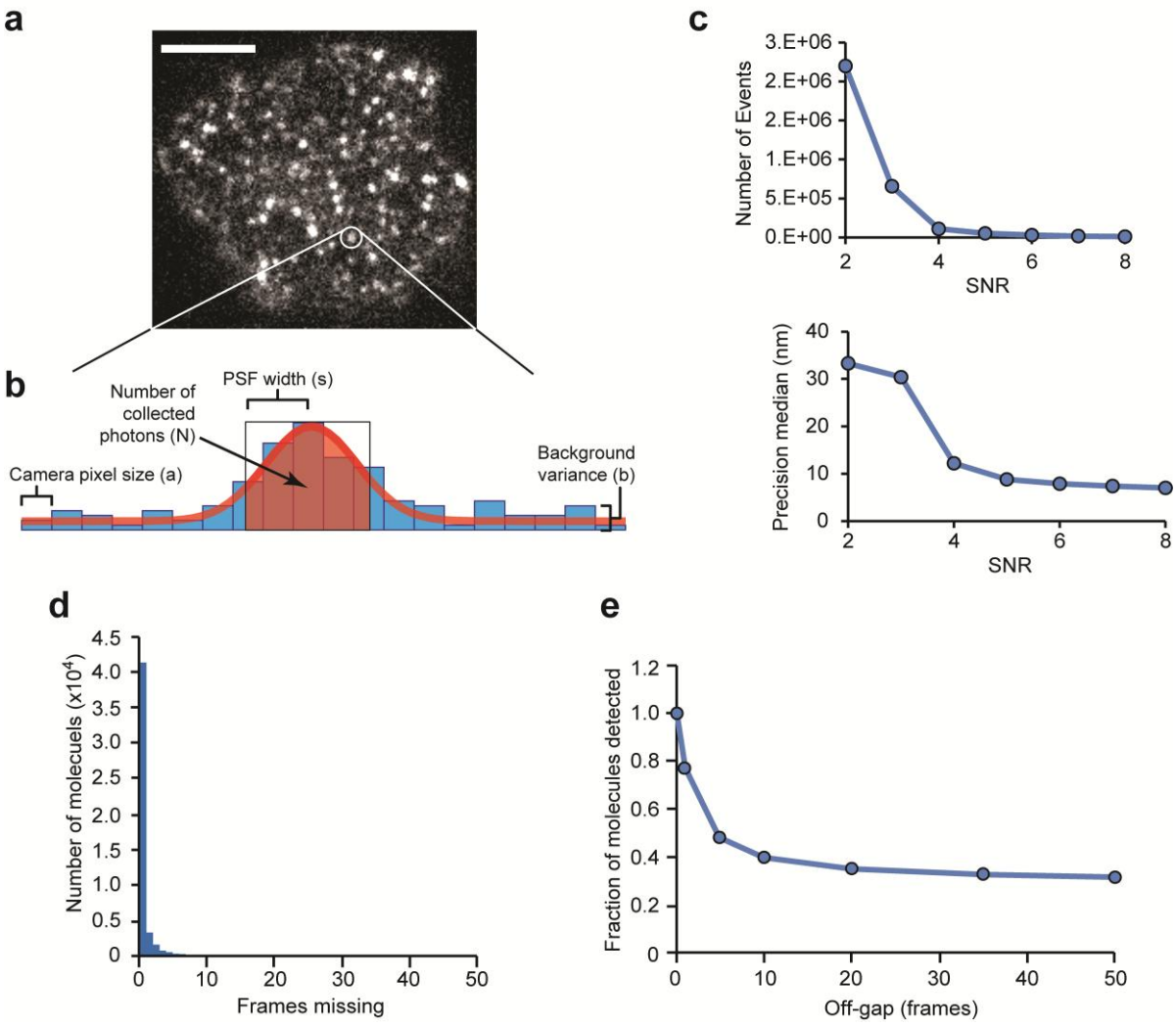

Supplementary Figure 1 Identification of single molecules for generating PALM and dSTORM images. (**a**) PALM image of Lat-mEos2 expressed in Lat-deficient JCaM2 cells. A single-molecule PSF is highlighted. Scale bar, 5 µm. (**b**) Schematic of a series of camera pixels containing a hypothetical PSF displaying the experimental parameters required to calculate the localization precision. (**c**) Total number of events detected and the median localization precision value for different SNR values for single-molecule discrimination. (**d**) The number of molecules in a representative dSTORM experiment that exhibit 'missing frames' in the detected fluorescence and are therefore potentially re-excited. (**e**) Number of detected molecules in a typical dSTORM experiments as a function of the off-gap. The off-gap defines the time period (in frames) in which fluorescent events that localize to the same area are summed and counted as one molecule.

Nature Immunology doi:10.1038/ni.2049

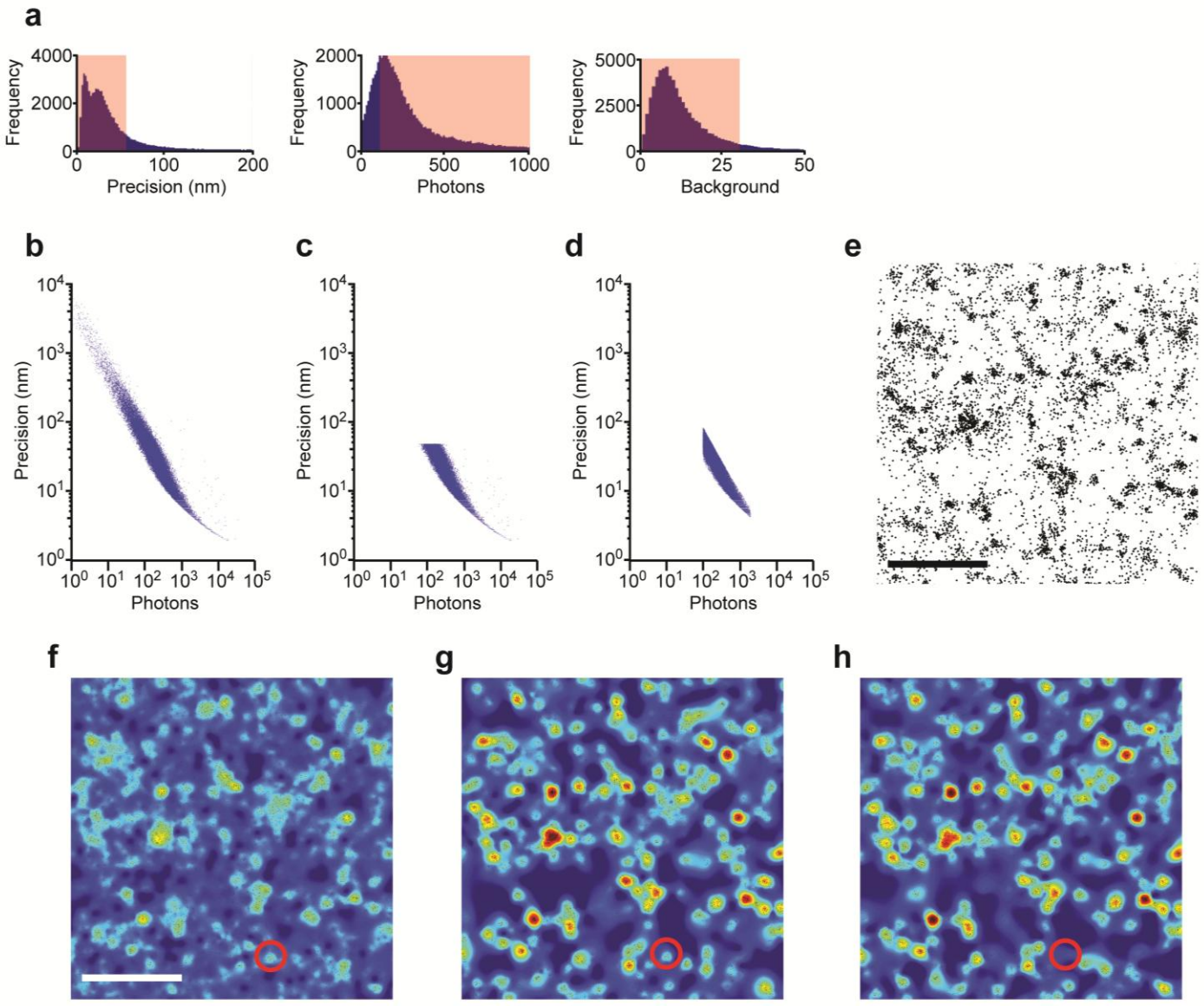

Supplementary Figure 2 Analysis of PALM and dSTORM images with local point pattern analysis and cluster thresholding. (**a**) Histograms of precision, photon counts and background for a representative PALM image of Lat-mEos2 expressed in JCaM2 cells. Red shaded areas highlight events that are included after thresholding. (**b-d**) Precision *versus* photon count plot for the entire data series (**b**), equivalent plot for data after thresholding by localization precision (Δx<50 nm) (**c**), and for data thresholded by photon count (N=100-2000) and background (b<30) (**d**). (**e-g**) 2-D point-pattern of particle coordinates for non-thresholded data (**e**). Cluster map of raw data (**f**) and after cropping by precision (**g**) and after cropping by photon count and background (**h**). Scale bars, 1 µm.

Nature Immunology doi:10.1038/ni.2049

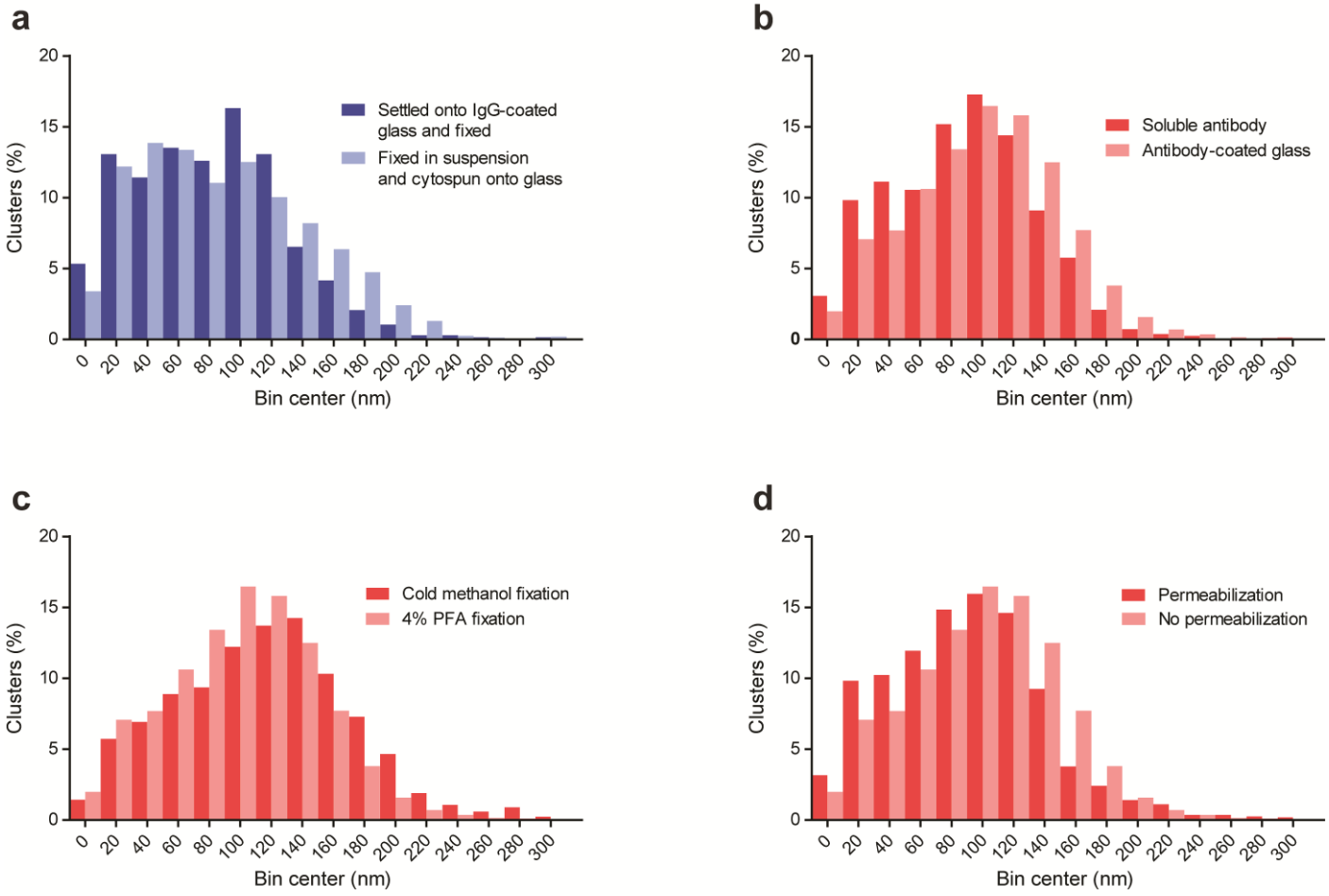

Supplementary Figure 3 Effect of sample preparation on Lat-mEos2 clustering in JCaM2 cells. (**a**) Distribution of Lat cluster sizes in resting JCaM2 cells that were either fixed in suspension and cyto-spun onto bare glass or allowed to settle onto glass coated with IgG antibodies which do not cause T cell activation and fixed as adherent cells. (**b**) Distribution of Lat cluster sizes for cells activated in suspension by soluble antibodies (anti-CD3 and anti-CD28) and cyto-spun onto bare glass and cells activated by antibody-coated glass coverslips. (**c**) Comparison of Lat cluster sizes in activated cells fixed with 4% PFA for 30 min and activated cells fixed with 0.1% cold methanol for 1 min. (**d**) Comparison of Lat cluster sizes in activated cells before and after permeabilization with lysolecithin (100 µg/mL). Data were obtained by analyzing 6 (**a**), 13 (**b**), 22 (**c**), and 20 (**c**) PALM image regions with local point pattern analysis and applying a cluster threshold.

Nature Immunology doi:10.1038/ni.2049

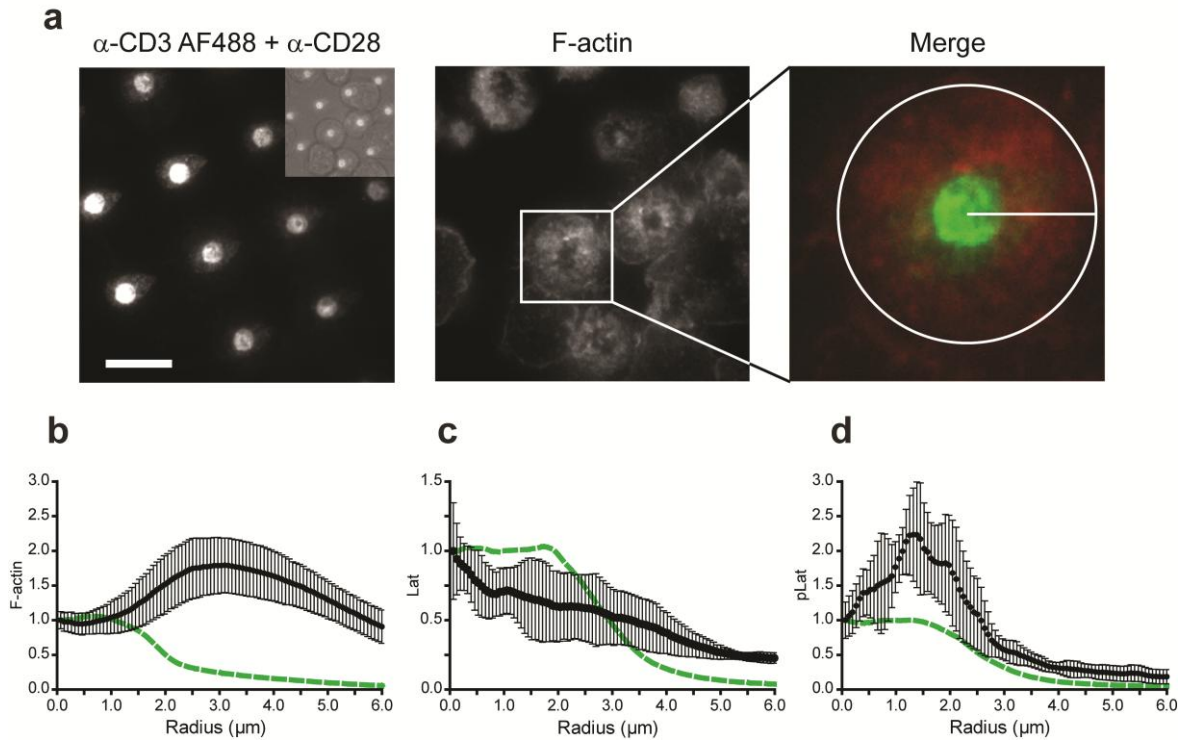

Supplementary Figure 4: Analysis of radial intensity profiles of TIRF images of T cells on micro-patterned surfaces. (**a**) Micro-patterned surfaces were constructed with AF488-conjugated anti-CD3 and anti-CD28 antibody dots 4 μm in diameter. After incubating Lat-expressing wild-type Jurkat cells with micro-patterned surfaces for 10 min at 37˚C, immunostaining was performed against F-actin using phalloidin, Lat and pLat and TIRF images acquired. Ring-integrated (radial) intensity profiles were determined for each TIRF image for a 6.0 μm radius circle center-aligned to the AF488 spot. Scale bar, 10 μm. (**b-d**) Radial intensity distributions of F-actin (**b**), Lat (**c**) and p-Lat (**d**) in Jurkat cells activated with micro-patterned surfaces. Intensity profiles were measured on 8 dots (p-Lat) or 11 dots (F-actin and Lat) and data are mean and standard deviation. The intensity profile of the anti-CD3/anti-CD28 antibodies is indicated by green lines.

Nature Immunology doi:10.1038/ni.2049

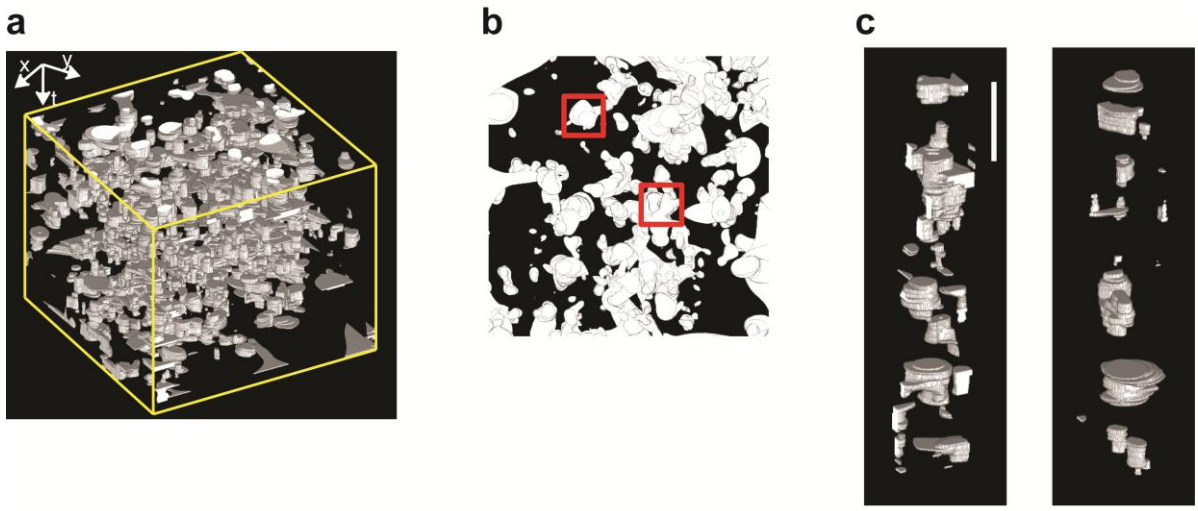

Supplementary Figure 5 Analysis of a Lat cluster map movie obtained with live cell PALM imaging. (**a**) 3D stack of cluster Lat cluster maps with time in the vertical dimension. (**b**) The same stack rotated and viewed *en face* (time projection) shows regions of the membrane where Lat clusters appeared during activation (white areas) as well as regions at which no Lat clusters were observed (black areas). (**c**) Two x-y regions of interest (red squares in (**b**)) over the course of activation with multiple Lat clusters appearing at the same site. Scale bar, 1 min.

Nature Immunology doi:10.1038/ni.2049

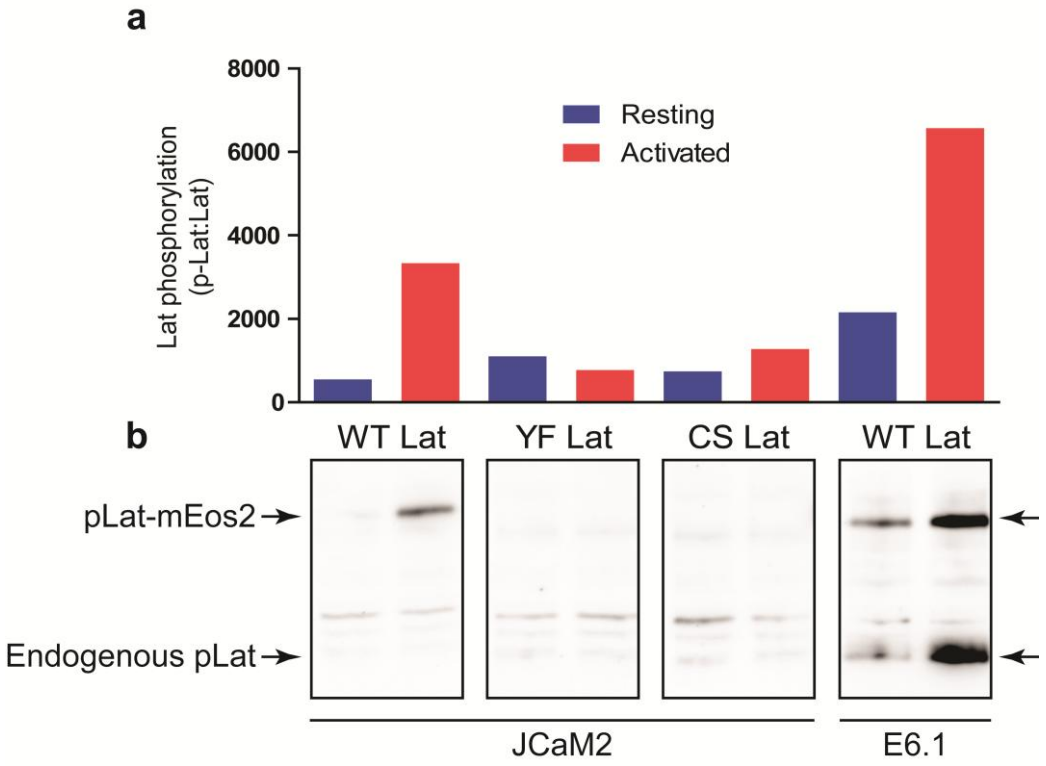

Supplementary Figure 6 Quantification of Lat phosphorylation by immuno-blotting. (**a**, **b**) Phosphorylation of wild-type and mutant Lat-mEos2 in resting and activated JCaM2 cells and wild-type, endogenous Lat in resting and activated JCaM2 Jurkat cells (**a**) determined by immuno-blotting (**b**). YF Lat is a mutant deficient in phosphorylation and lacks all nine tyrosine phosphorylation site. CS Lat is a mutant deficient in vesicular transport and lacks the two palmitoylation sites (CS Lat).

Nature Immunology doi:10.1038/ni.2049

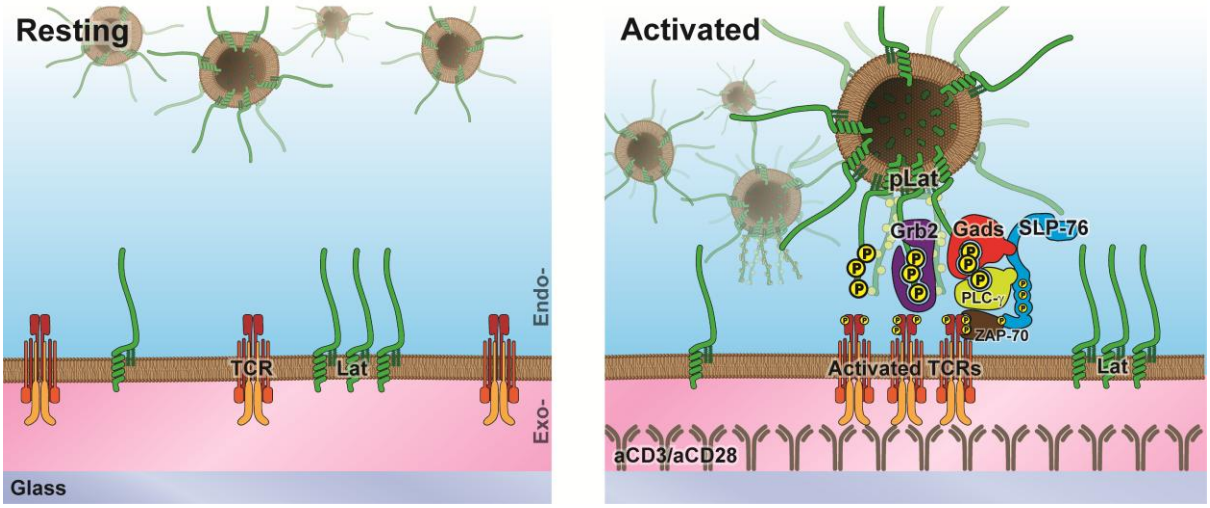

Supplementary Figure 7 Vesicular model of Lat signaling. In the resting T cells, Lat resides in two distinct pools: at the cell membrane and within a vesicular pool[6]. Within the plasma membrane, a proportion of Lat molecules resides in clusters independent of TCR activation[7]. When the TCR is activated, vesicular Lat is recruited to the immunological synapse[8] resulting in an increase in Lat clusters detected by super-resolution fluorescence microscopy. It is this vesicular Lat population which accounts for the increase in Lat density on the cell surface, the appearance of new Lat clusters, and the formation of phosphorylated Lat signaling networks upon TCR activation. Whether Lat vesicles are required to fuse with the plasma membrane for signaling and receptor internalization is currently not known. However, pre-existing Lat clusters on the cell surface do not participated in early T cell signaling events. SLP76 is Src-homology-2-domain-containing leukocyte protein of 76 kDa; Grb2 is growth factor receptor-bound protein 2 (Grb2), GADS is Grb2-homologous adapter (GADS) and PLCγ is phospholipase C gamma.

Nature Immunology doi:10.1038/ni.2049

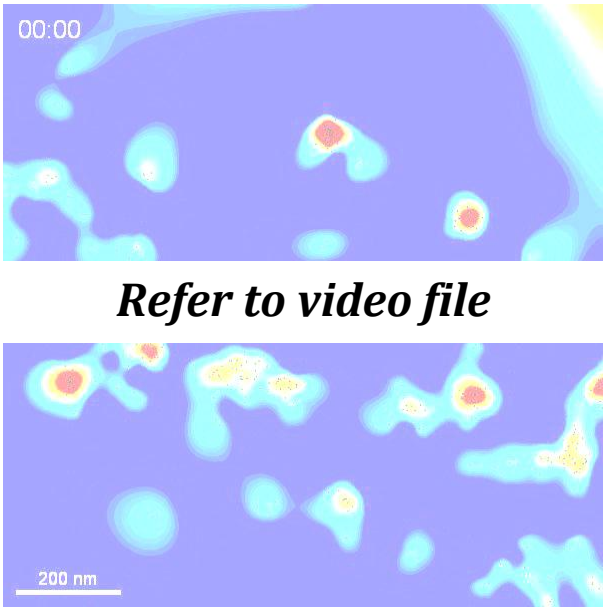

Supplementary Movie 1 Lat cluster map movie. Live cell PALM images of Lat-mEos2 in an activated JCaM2 cell were converted into a cluster map movie. Each movie frame is a cluster map derived from 3000 PALM acquisition images, advancing by 250 acquisition images, or 2.9 s, with each consecutive movie frame. The JCaM2 cell was deposited onto an anti-CD3 and anti-CD28 antibody coated glass coverslip and allowed to settle onto the surface. PALM acquisition commenced one minute later for a further ten minutes.

Nature Immunology doi:10.1038/ni.2049